A progeria mutation reveals functions for lamin A in nuclear assembly, architecture, and chromosome organization

Pekka Taimen[a,1], Katrin Pfleghaar[a,1], Takeshi Shimi[a], Dorothee Möller[b], Kfir Ben-Harush[c], Michael R. Erdos[d], Stephen A. Adam[a], Harald Herrmann[b], Ohad Medalia[c], Francis S. Collins[d,2], Anne E. Goldman[a], and Robert D. Goldman[a,2]

[a]Department of Cell and Molecular Biology, Feinberg School of Medicine, Northwestern University, Chicago, IL 60611; [b]Division of Molecular Genetics, German Cancer Research Center, D-69120 Heidelberg, Germany; [c]Department of Life Sciences, Ben Gurion University and the NIBN, Beer-Sheva 84120 Israel; and [d]Genome Technology Branch, National Human Genome Research Institute, Bethesda, MD 20892

Contributed by Francis S. Collins, October 15, 2009 (sent for review September 10, 2009)

Numerous mutations in the human A-type lamin gene (*LMNA*) cause the premature aging disease, progeria. Some of these are located in the α-helical central rod domain required for the polymerization of the nuclear lamins into higher order structures. Patient cells with a mutation in this domain, 433G>A (E145K) show severely lobulated nuclei, a separation of the A- and B-type lamins, alterations in pericentric heterochromatin, abnormally clustered centromeres, and mislocalized telomeres. The induction of lobulations and the clustering of centromeres originate during postmitotic nuclear assembly in daughter cells and this early G1 configuration of chromosomes is retained throughout interphase. In vitro analyses of E145K-lamin A show severe defects in the assembly of protofilaments into higher order lamin structures. The results show that this central rod domain mutation affects nuclear architecture in a fashion distinctly different from the changes found in the most common form of progeria caused by the expression of LAΔ50/progerin. The study also emphasizes the importance of lamins in nuclear assembly and chromatin organization.

centromere | chromatin | Rabl | senescence | telomere

The lamins are type V intermediate filament (IF) proteins comprising the major structural components of the nuclear lamina, the fibrous meshwork underlying the inner nuclear membrane (1). They are major determinants of nuclear size and shape and are involved in essential functions such as DNA replication and transcription (1). Lamins A (LA) and C (LC) are alternatively spliced products of the *LMNA* gene, whereas lamins LB1 and LB2 are encoded by *LMNB1* and *LMNB2*. Structurally, the lamins have a conserved central α-helical rod domain flanked by globular head and tail domains. The central rod is responsible for the formation of in-parallel and in-register coiled-coil dimers, the building blocks of lamin polymers. In vitro, lamin dimers form head-to-tail chains, which further interact laterally in an anti-parallel orientation to form highly ordered paracrystals (PCs) (2). However, little is known about the assembly of lamins into higher order structures in vivo.

There are >250 mutations in human *LMNA* causing a wide range of diseases [for detail, see http//www.umd.be/LMNA/ and (3)]. Among these is the rare premature aging disease, Hutchinson–Gilford progeria syndrome (HGPS). HGPS children typically appear normal at birth, but show growth retardation before the age of 2 years. Further manifestations include loss of hair, lipodystrophy, sclerodermatous skin, osteolysis, and progressive atherosclerosis leading to death at an average age of 13 years due to myocardial infarcts and strokes (4). Most HGPS patients carry the 1824C>T mutation (G608G), which activates a cryptic splice site resulting in the expression of LA with 50 amino acids deleted near its C terminus (LAΔ50/progerin) (5). As a result, LAΔ50/progerin remains permanently farnesylated (6, 7), and its accumulation in patients' cells is correlated with the loss of heterochromatin and changes in histone methylation (1).

In addition to 1824C>T, there are 21 other *LMNA* mutations causing progeria (http://www.umd.be/LMNA/). Some of these are located in the central rod domain, where they could directly impact the assembly of lamins into dimers and higher order structures. Here, we have studied the alterations in nuclear architecture and chromatin organization in one of these mutations, 433G>A (E145K), located in segment 1B of the central rod domain of LA/C (5). A patient bearing this mutation showed earlier onset cardiovascular defects, only partial loss of hair and ample s.c. fat (5). We show that fibroblasts derived from an E145K patient have severely misshapen nuclei and multiple defects in chromatin organization as reflected by centromere clustering and an abnormal distribution of telomeres throughout the cell cycle. These abnormalities are established during cell division as nuclei assemble in daughter cells. The results demonstrate that the nuclear changes in E145K progeria cells are significantly different from those seen in cells expressing LAΔ50/progerin, and they also emphasize the essential role of lamins in establishing and maintaining nuclear architecture.

Results

Dermal fibroblasts from an E145K progeria patient (E145K cells) contain severely lobulated nuclei (Fig. 1*A* and Fig. S1*A*). Approximately 32% (n = 300) of the nuclei showed three or more lobules (multilobulated) by passage (p) 9, and by p13 this increased to approximately 69% (n = 300) (Fig. S1*B*). Normal fibroblasts (control cells) were essentially free of lobules [≈1% (n = 300), p15] (Fig. S1*B*). Contour ratio analyses confirmed that E145K nuclei had very different shapes compared to controls (Fig. S1*C*). Furthermore, the lobulated nuclei in E145K cells did not regain normal nuclear shapes following 48-72 h of treatment with the farnesyl transferase inhibitor FTI-277 (Fig. S2), which is distinctly different from cells expressing LAΔ50/progerin (8, 9).

Immunofluorescence revealed that LA/C were concentrated in the lamina with lower levels in the nucleoplasm in both E145K nuclei and controls (Fig. 1*A*). However, in multilobulated E145K nuclei there was an overall reduction in LB1 and LB2, which were barely detectable in the outermost regions of the lamina delimiting the lobules (Fig. 1*A*). Any detectable B-type lamins

Author contributions: P.T., K.P., T.S., S.A.A., H.H., O.M., F.S.C., and R.D.G. designed research; P.T., K.P., T.S., D.M., K.B.-H., M.R.E., H.H., O.M., and A.E.G. performed research; M.R.E. and F.S.C. contributed new reagents/analytic tools; P.T., K.P., T.S., D.M., K.B.-H., M.R.E., S.A.A., H.H., O.M., F.S.C., A.E.G., and R.D.G. analyzed data; and P.T., K.P., T.S., S.A.A., H.H., O.M., A.E.G., and R.D.G. wrote the paper.

The authors declare no conflict of interest.

Freely available online through the PNAS open access option.

[1]P.T. and K.P. contributed equally to this work.

[2]To whom correspondence may be addressed: E-mail: r-goldman@northwestern.edu or francis.collins@gmail.com.

This article contains supporting information online at www.pnas.org/cgi/content/full/0911895106/DCSupplemental.

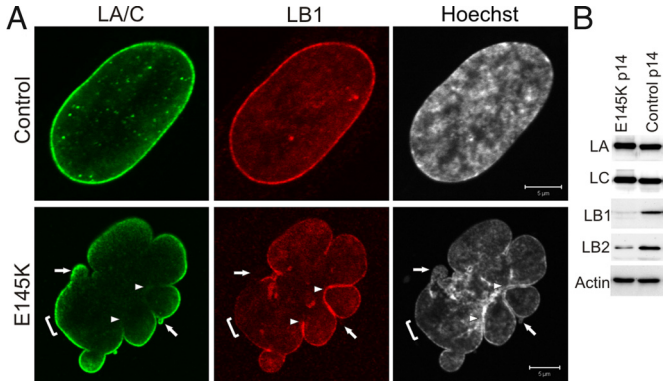

Fig. 1. Lamin alterations in E145K cells. (*A*) E145K (p11) and control cells (p19) were stained with anti-LA/C, anti-LB1, and Hoechst. Mid-plane confocal sections show extensive lobulation of the NE in E145K cells. LA/C is associated mainly with the outer region of the lobules (bracket), which stain weakly for LB1 and surround a euchromatic region as indicated by weak staining with Hoechst. Arrows indicate small blebs containing LA/C, but no detectable LB1. LB1 is associated with the heterochromatic proximal regions of the lobules, which contain little LA/C (arrowheads). (Scale bars, 5 μm.) (*B*) Immunoblotting analysis of E145K and control cells at p14. The amount of LB1 and to a lesser extent of LB2 is reduced in E145K cells, while LA and LC are expressed at levels comparable to controls.

were enriched in the proximal regions of the lobules frequently in close association with heterochromatin, where little or no LA/C could be detected (Fig. 1*A*). Approximately 15% ($n = 300$) of the multilobulated E145K nuclei also had smaller nuclear envelope (NE) "blebs" enriched in LA/C, but devoid of LB1/2 (Fig. 1*A*) (10, 11). Immunoblotting confirmed a significant reduction in the amount of LB1, and to a lesser extent LB2, in E145K cells relative to controls (Fig. 1*B*). Emerin, an inner nuclear membrane protein, and nuclear pore complexes (NPCs), were located in all regions of the nuclear surface in the multilobulated E145K nuclei, extending into the clefts formed by adjacent lobules (Fig. S3 *A* and *B*).

Transmission electron microscopy (TEM) revealed that the lobules of E145K nuclei contained a distinct lamina and a significant reduction in peripheral heterochromatin compared to controls (Fig. S3*C*) (10). In agreement with the fluorescence observations, the heterochromatin in the multilobulated nuclei was more pronounced in regions where the deep invaginations of adjacent lobules appeared to merge (Fig. S3*C*).

The reduction in heterochromatin in lobules suggested a loss of epigenetic marks as previously described in patient cells expressing LAΔ50/progerin (12). Immunofluorescence revealed that histone H3 trimethylated at lysine 9 (H3K9me3), a mark for pericentric constitutive heterochromatin and repressed euchromatin, was concentrated in the same central region that stained intensely with Hoechst (Fig. 2*A*). This is different from normally shaped E145K nuclei or nuclei in normal cells where this mark is enriched in the nuclear periphery and perinucleolar region (Fig. 2*A*). Staining for H3K27me3, a mark for facultative heterochromatin, showed no obvious differences between multilobulated and normally shaped nuclei in E145K or control cells (Fig. 2*A*).

Immunostaining with CREST antibody (13) revealed that approximately 80% ($n = 100$) of multilobulated E145K nuclei contained abnormally clustered centromeres in the region of intense Hoechst staining (Fig. 2*B*). Similar centromere clustering occurred in only approximately 6% ($n = 100$) of normally shaped E145K nuclei and approximately 3% ($n = 200$) of control nuclei. The majority of normally shaped nuclei had centromeres distributed throughout the nucleoplasm, with some closely associated with the lamina (Fig. 2*B*). We also determined telomere positioning relative to centromeres with a telomeric FISH probe and immunostaining with CREST and LA antibodies. In normally shaped E145K and control cell nuclei, telomeres and centromeres were found interspersed throughout the nucleoplasm (Fig. 2*C*). In multilobulated E145K nuclei, many telomeres were no longer interspersed with centromeres, but were found at varying distances from the clustered centromeres and were frequently associated with the lamina (Fig. 2*C*).

To determine if the changes in nuclear architecture are due directly to E145K-LA, FLAG-tagged E145K-LA (FLAG-E145K-LA) was expressed in HeLa cells (Fig. 3*A*). After 24 h, 2.7 ± 1.4% of the transfected cells were multilobulated, increasing to 18 ± 3% and 37 ± 9% at 48 and 72 h posttransfection (p.t.), respectively. Control cells expressing wild-type LA (FLAG-WT-LA) were rarely lobulated at 72 h p.t. (2.4 ± 0.8%) (Fig. 3*A*). The multilobulated HeLa nuclei expressing FLAG-E145K-LA also contained centrally clustered centromeres as indicated by CREST staining (Fig. 3*A*), and few telomeres were interspersed with the centromeres (Fig. 3*B*). To verify this, the distribution of the telomeres was quantified in Z-stacks of confocal images revealing that 16 ± 3 telomeres ($n = 14$) were associated with the lamina region in FLAG-WT-LA expressing HeLa cells, whereas in FLAG-E145K-LA expressing cells, an average of 35 ± 6 telomeres ($n = 10$ nuclei) were associated with the lamina. These results demonstrate that the expression of E145K-LA has a profound effect on the organization of chromatin.

To test whether this atypical chromatin organization affects DNA replication, double replication labeling of E145K patient cells was used (11, 14). The number of E145K cells with both early and late replication foci (≈9%, $n = 538$) was significantly decreased compared to controls (≈27%, $n = 528$) at p13. Furthermore, the distribution of early and late replication foci was altered in E145K cells. In controls, early replication foci were distributed throughout the nucleoplasm, while mid-to-late replication took place both in the lamina region and in large nucleoplasmic foci. Many of the latter coaligned with centromeres (Fig. 4). In contrast, the majority of the early replicating foci were in lobulated regions in E145K nuclei, while many late replicating foci were concentrated in the central region containing clustered centromeres (Fig. 4). These data suggest that although chromatin is disorganized, the overall timing of early and late replication was not affected. Analysis of other proliferation markers revealed that approximately 6% of E145K cells (p13, $n = 300$) and approximately 26% of control cells (p13, $n = 300$) showed typical S phase PCNA patterns (15); while approximately 9% of E145K (p13, $n = 200$) and approximately 42% of control (p15, $n = 200$) cells were positive for the Ki-67 antigen (16), suggesting that the mutant cells had reduced proliferative capacity.

The E145K cells also senesce prematurely compared to controls as assayed by senescence-associated β-galactosidase (17). While approximately 8% ($n = 620$) of control cells were positive for β-galactosidase at p17, approximately 23% ($n = 743$) of E145K cells were positive at p14. There was also a strong correlation between senescence and nuclear lobulation. This was supported by the findings that approximately 4% ($n = 208$) of E145K cells with normally shaped nuclei, approximately 12% with one or two nuclear lobules ($n = 163$), and approximately 39% with multilobulated nuclei ($n = 372$) were positive for β-galactosidase (Fig. S4).

To determine when multilobulated nuclei with clustered centromeres form, we carried out live cell imaging studies in HeLa cells stably expressing YFP-tagged centromere protein A (YFP-CENP A). When these cells were cotransfected with mCherry-WT-LA and either FLAG-E145K-LA or FLAG-WT-LA, approximately 99% of the mCherry-WT-LA positive cells also expressed FLAG-tagged LA at 72 h p.t. This multiple transfection was necessary as EGFP-E145K-LA did not induce the

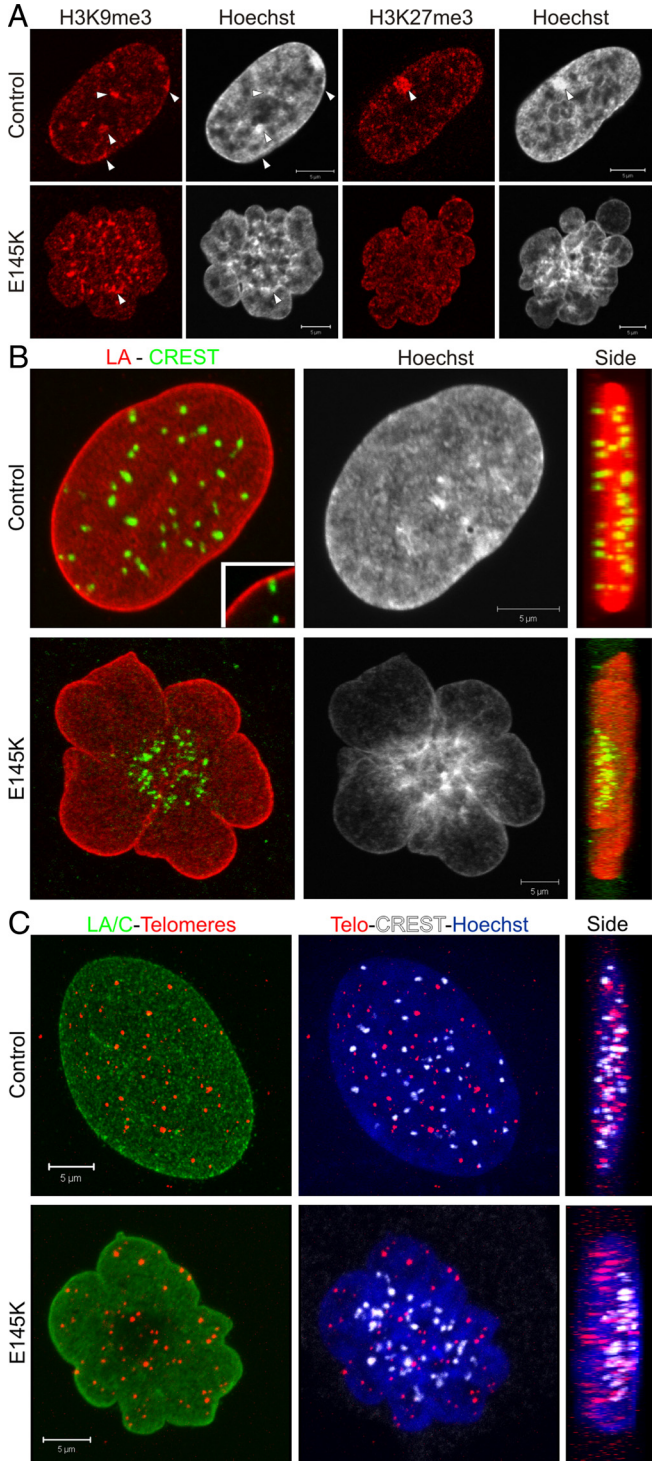

Fig. 2. Mislocalization of heterochromatin, centromeres, and telomeres in E145K cells. (*A*) E145K (p11) and control cells (p11) were stained with either anti-H3K9me3 or anti-H3K27me3 and Hoechst. Mid-plane confocal sections show enrichment of H3K9me3 in the central region of the nucleus in E145K cells (arrowhead), while it is enriched in the nuclear periphery and in perinucleolar regions in controls (arrowheads). H3K27me3 is distributed throughout the nucleus in both cells and enriched in the Xi in female control cells (arrowhead). (Scale bars, 5 μm.) (*B*) E145K (p13) and control cells (p15) were stained with anti-LA, CREST antiserum, and Hoechst. Maximum projections of series of z-sections spanning the entire nucleus and side projections are shown. Centromeres are clustered in the central region of the nucleus in E145K cells, while they are either closely associated with the peripheral lamina region or elsewhere in the nucleoplasm in control cells. *Inset* shows an example of the close association of one centromere with the lamina in a single confocal section. (Scale bars, 5 μm.) (*C*) E145K and control cells were stained with anti-LA/C, CREST antiserum, and Hoechst. A FISH probe was used to visualize telomeres. Maximum projections of series of z-sections spanning the entire nucleus and side projections from merged images are shown. Centromeres and telomeres are distributed throughout the nuclei in control cells. In E145K cells centromeres are clustered in the middle of one region of the nucleus, while telomeres are more frequently associated with the peripheral lamina region. (Scale bars, 5 μm.)

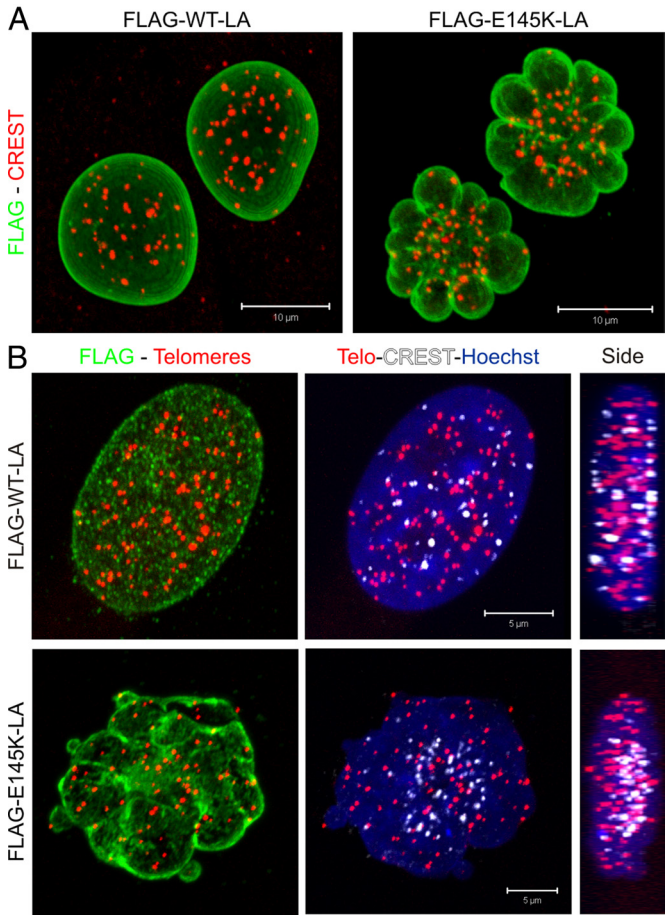

Fig. 3. Expression of FLAG-E145K-LA in HeLa cells induces nuclear lobulations and mislocalization of centromeres and telomeres. (*A*) HeLa cells were transfected with either FLAG-WT-LA or FLAG-E145K-LA for 72 h and stained with anti-FLAG and CREST antiserum. Maximum projections of series of z-sections spanning the entire daughter cell nuclei are shown. Note the extensive lobulation of the lamina and clustering of centromeres in FLAG-E145K-LA-expressing cells. (Scale bars, 5 μm.) (*B*) HeLa cells were transfected with either FLAG-WT-LA or FLAG-E145K-LA for 72 h, fixed, and stained with anti-FLAG, CREST antiserum, Hoechst, and a FISH probe to visualize telomeres. Maximum projections of z-sections and side projections are shown as above. Centromeres and telomeres are distributed throughout the nuclei in FLAG-WT-LA-expressing cells. In FLAG-E145K-LA-expressing cells centromeres and telomeres are less interspersed, and telomeres are more likely to be associated with the peripheral lamina region. (Scale bars, 5 μm.)

nuclear phenotype seen with FLAG-E145K-LA. The reason for this difference is unknown, but may be attributable to the larger size of the EGFP tag relative to FLAG. Live imaging of interphase and mitotic cells revealed no differences between the FLAG-WT-LA and FLAG-E145K-LA-transfected cells through early telophase (Fig. 5, Fig. S5, and Movies S1 and S2). However, approximately 59% ($n = 22$) of the FLAG-E145K-LA expressing cells entering mitosis with normally shaped nuclei, formed

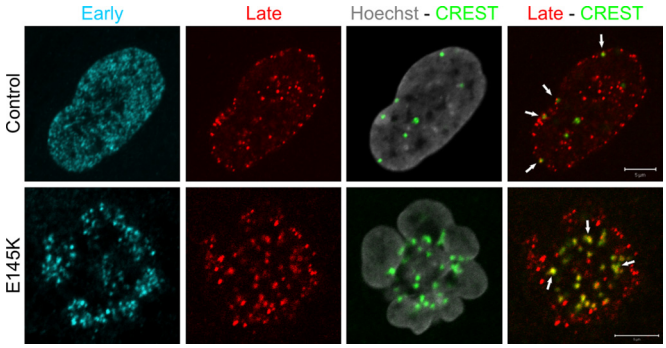

Fig. 4. Multilobulated E145K patient cells are capable of replicating their DNA despite the abnormal chromatin configuration. Double replication labeling assays (first pulse: IdU, 4 h Chase, second pulse: CldU) were carried out on E145K and control cells and subsequently stained with CREST antiserum and Hoechst. Single confocal sections showing both early and mid-to-late replication patterns are presented. In control cells, early replication foci are distributed throughout the nucleus, while mid-to-late replication foci are either found in association with the lamina region or deeper in the nucleoplasm. Some of the mid-to-late foci colocalize with CREST (arrows). In E145K cells early replication foci are enriched in lobules while many of the mid-to-late replication foci are concentrated in the central region of the nucleus with the clustered centromeres (arrows). (Scale bars, 5 μm.)

daughter cells with multilobulated nuclei and clustered centromeres (Fig. 5 and Movie S1). Centromere clustering was maintained for the entire period of observation up to 10 h following cytokinesis (Fig. 5). In contrast, newly divided cells expressing FLAG-WT-LA always formed normally shaped nuclei with a normal distribution of centromeres within 1-2 h into G1 ($n = 12$) (Fig. S5 and Movie S2). The multilobulated nuclei induced by FLAG-E145K-LA never reverted to normal shapes following mitosis. In fact, some cells with lobulated nuclei divided to form daughter cells with lobulated nuclei and clustered centromeres (Fig. S6*A*). This observation was supported by flow cytometric DNA content analysis, which showed no differences in the distribution of cells in different phases of the cell cycle between FLAG-WT-LA and FLAG-E145K-LA expressing cells at 72 h

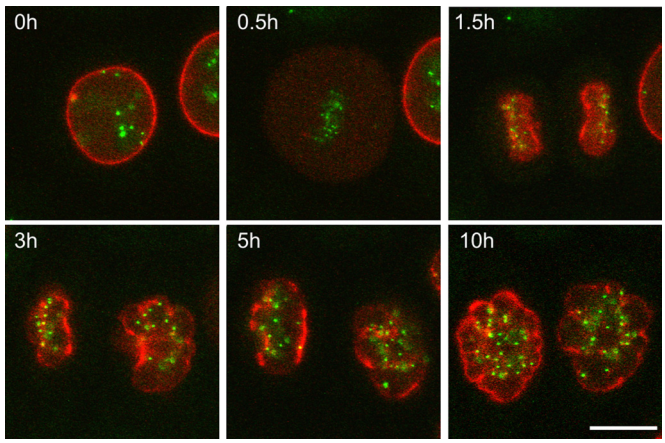

Fig. 5. FLAG-E145K-LA interferes with postmitotic nuclear assembly and centromere positioning in daughter cells. HeLa cells stably expressing YFP-CENP A (green) were transfected with FLAG-E145K-LA and mCherry-WT-LA (red) for 48-72 h. Cells with normally shaped nuclei were followed through mitosis and nuclear reassembly by using time-lapse imaging. A single confocal section is shown for each time point. mCherry-LA is localized normally during metaphase, anaphase, and telophase (0.5 to 1.5 h), but the daughter cells eventually show lobulated NE and clustered centromeres for up to 10 h. (Scale bar, 10 μm.)

p.t. (Fig. S7). Further confirmation that the nuclear shape changes induced by FLAG-E145K-LA require cell division was obtained by arresting cells in early S phase with aphidicolin (18). This treatment completely inhibited the formation of multilobulated nuclei (Fig. S6*B*).

The location of the E145K mutation in the central rod domain of LA/C suggested that a disruption of normal lamin assembly might be responsible for the changes in nuclear architecture. In vitro analyses of LA complex formation by analytical ultracentrifugation (AUC) (19, 20) showed that both E145K-LA and LAΔ50/progerin form dimers that are indistinguishable from WT-LA (Fig. S8*A*). To initiate assembly of higher order structures, solutions of dimers were diluted into assembly buffer, and samples were prepared at different times for TEM analysis. Both WT-LA and LAΔ50/progerin formed extended arrays of filaments of varying diameter after 10 min (Fig. 6). In contrast, E145K-LA formed interconnected fibrous strands, which aggregated into globular disorganized assemblies. The structures formed by WT-LA and LAΔ50/progerin at 10 min were transient states leading to larger and more ordered arrays after 30 min (Fig. S8*B*). These structures exhibited a characteristic 24-nm axial repeat reflecting the lateral anti-parallel association of head-to-tail chains of dimers. In contrast, some thin E145K-LA filaments appeared after 30 min, but no axial repeats could be detected (Fig. S8*B*).

The end point of the in vitro assembly of lamins is the formation of PCs. Due to the thickness of PCs, we determined their structure in unfixed preparations embedded in amorphous ice by using cryo-electron tomography (cryo-ET) and 3-D image processing (21). Slices (x-y) of 60-nm-thick sections through reconstructed volumes of typical WT-LA and LAΔ50/progerin PCs showed regular arrays of protofilaments exhibiting the expected 24-nm repeats of dimeric tail domains along the ordered structures (Fig. 6). In contrast, E145K-LA formed atypical PCs with no obvious longitudinal repeat patterns demonstrating that the lateral association of protofilaments was abnormal (Fig. 6).

Since previous studies showed that LAΔ50/progerin is less soluble than WT-LA (22), the solubility of E145K-LA was also tested. Sequential extraction of FLAG-E145K-LA and FLAG-WT-LA expressing HeLa cells, however, showed no differences in the solubilities of WT-LA and E145K-LA, suggesting that both assembled into stable structures under these conditions (Fig. S9).

Discussion

The E145K progeria mutation in LA/C alters lamin structure and assembly, inducing profound changes in nuclear architecture, a reduction in B-type lamin expression, and premature senescence. In contrast to the more common LAΔ50/progerin mutation, the E145K mutation does not alter the posttranslational processing of the C terminus, which explains why its impact on nuclear shape is not reversed by FTI treatment (6, 7). The E145K mutation also causes the clustering of centromeres and their associated H3K9me3, but it does not alter the distribution of H3K27me3 heterochromatic mark. In contrast, LAΔ50/progerin alters both of these epigenetic marks, and the association between H3K9me3 and some centromeres is lost (12). In addition, the E145K mutation has no obvious impact on the distribution of NPCs, which is in contrast to the abnormal distribution of NPCs in LAΔ50/progerin expressing cells (10). Therefore, distinctly different cellular phenotypes are induced by these two mutations causing premature aging.

The nuclear phenotypes induced by E145K-LA and LAΔ50/progerin suggest that these mutations may cause progeria by altering the structure of the lamina, albeit by different mechanisms. In support of this, the E145K mutation has a deleterious effect on LA polymerization into higher order structures in vitro;

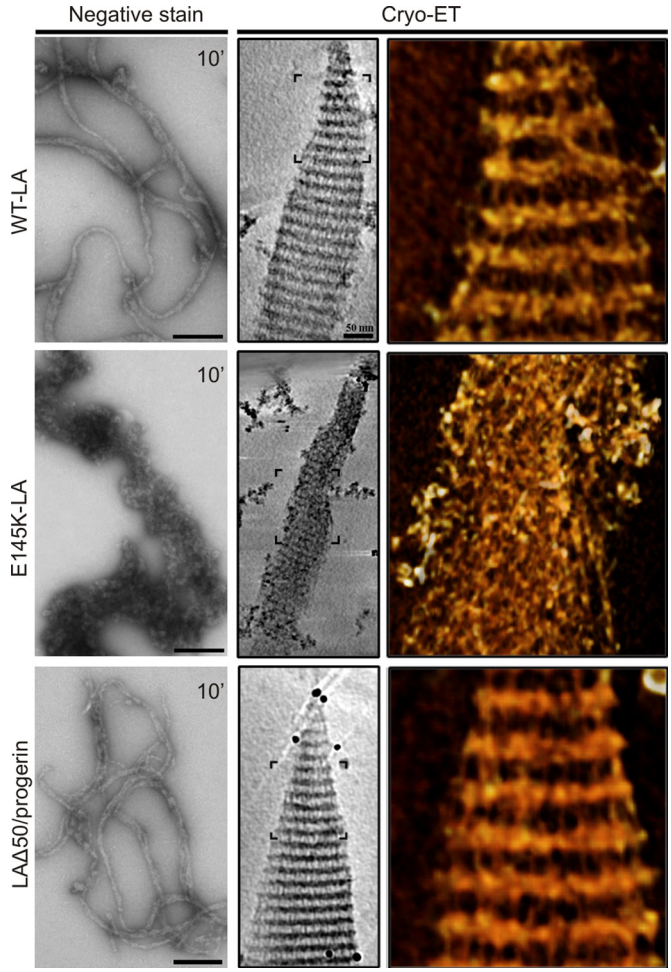

Fig. 6. Structural analysis of filaments and PCs assembled from WT-LA, E145K-LA, and LAΔ50/progerin. Bacterially expressed and purified WT-LA, E145K-LA, and LAΔ50/progerin were allowed to self-assemble into filaments and PCs in vitro and analyzed by TEM. Negatively stained images show that filaments of varying diameters assembled from WT-LA and LAΔ50/progerin are well ordered after 10 min, while those assembled from E145K-LA are disorganized. For cryo-ET, 60-nm-thick x-y slices along the z-axis through tomograms of PC assembled from WT-LA, E145K-LA, and LAΔ50/progerin are shown. Pseudo-colored higher magnification images show volume rendering views of 30-nm-thick tomographic slices of the marked regions. Both WT-LA and LAΔ50/progerin PCs show similar repeat patterns at low magnification. In contrast the E145K-LA PC is significantly less well ordered. This is emphasized at higher magnification, which shows that the protofilaments in PCs assembled from WT-LA and LAΔ50/progerin are well ordered, while the lateral interactions of protofilaments in PC assembled from E145K-LA are disordered. [Scale bars, 0.2 μm (*Left*) and 50 nm (*Middle*).]

whereas the polymerization of LAΔ50/progerin, whose amino acid sequence is significantly different from both WT-LA and E145K-LA, appears normal. Thus, it is likely that it is the abnormal association and accumulation of permanently farnesylated LAΔ50/progerin at the NE membrane that disrupts the normal functions of the lamina in the LAΔ50/progerin patients (6–10, 12), whereas in the case of E145K patients, it is the abnormal polymerization of LA that prevents the assembly of a normal lamina structure. Ultimately such differences could help to explain the different phenotypes seen in progeria, as well as other laminpathy patients bearing different mutations in *LMNA*.

The impact of alterations in the E145 residue are most likely attributable to its location in subdomain 1B of the central rod domain of LA/C. Similarly, mutations in the central rod domain of cytoskeletal IF proteins, such as desmin, keratins, and vimentin, have severe consequences for filament structure and function and cause variety of diseases including skeletal and cardiac myopathies (23), skin blistering diseases (24), and cataracts (25). The E145 residue is in an e position of one of the six heptads within the 42-amino acid sequence that is unique to lamins, and it is predicted to be solvent exposed rather than residing in the coiled-coil interface. Although substituting lysine for glutamic acid at residue 145 does not alter dimer assembly as shown by AUC analysis, it does alter the normal alignment of protofilaments into filaments and PCs (2). In further support of this, a mutation in the corresponding site of *Caenorhabditis elegans* lamin (*lmn-1*), Q159K, alters the structure of in vitro assembled filaments (21, 26).

As we previously observed in LAΔ50/progerin expressing patient fibroblasts (10), nuclear shape defects accumulate as a function of passage number in E145K cells suggesting a dominant negative effect of this mutant LA/C protein. In addition, live imaging of HeLa cells expressing FLAG-E145K-LA and treatment with aphidicolin demonstrate that lobulation is established during postmitotic nuclear assembly. Therefore, it is likely that the assembly of the lamina during late telophase/early G1 is severely affected once the relative amount of the E145K mutant lamin reaches a critical level. It is also relevant to note that the E145K mutation is present in both LA and LC, whereas the 1824C>T (LAΔ50/progerin) mutation does not affect the sequence of LC.

Within interphase nuclei, chromosomes are organized into "territories," with gene-rich chromosomes more likely to be internally located and gene-poor chromosomes more likely to be at the nuclear periphery (27, 28). Individual chromosomes are typically oriented with their centromeres situated in the nuclear periphery (29), while telomeres are distributed throughout the nucleoplasm (30). In the multilobulated E145K, nuclei chromosomes are organized with their centromeres clustered in one region. This is reminiscent of the "Rabl configuration," a polarized chromosome configuration found in the interphase nuclei of *Drosophila* and certain plant cells (31). The Rabl configuration originates in anaphase, when sister centromeres separate as chromosomes move to the spindle poles, and it is retained throughout interphase until the next mitosis (31). The polarized configuration of chromosomes in E145K cells is also established during and immediately following mitosis and persists throughout the G1 and S phases of the cell cycle (Fig. S10). Therefore, the expression of LA/C with the E145K mutation inhibits the normal reorganization of interphase chromosome territories in daughter cells in early G1, most likely due to the formation of an abnormal lamina structure. In support of this, it has been shown that lamins interact with mitotic chromosomes (32–34) and that their assembly at the surface of chromosomes is crucial for postmitotic nuclear formation (35, 36). It is also possible that the E145K mutation interferes with the lamin binding to matrix attachment regions of DNA (37) or interactions with other chromatin associated lamin-binding proteins such as histones, LAP2α, BAF (33), and/or SUN2 (38). Even though we do not know the exact mechanisms responsible for the impact of the E145K mutation, the results of this study provide important insights into the role of lamins in the spatial and temporal organization of chromosomes throughout the cell cycle.

In summary, the E145K mutation causes changes in lamin polymerization and assembly, resulting in a cellular phenotype that is distinctly different from LAΔ50/progerin expressing cells. Common features shared by these two very different mutations are that they both result in the down-regulation of B-type lamins (39) and premature replicative senescence (40). These factors may represent common denominators in the etiology of the different forms of premature aging disease. Interestingly, the expression of LAΔ50/progerin in human adult mesenchymal

stem cells also alters their differentiation pathways (41), which may ultimately explain why mesenchymal tissues are those most affected in HGPS. Whether E145K-LA also leads to a similar failure in stem cell differentiation remains to be determined.

Materials and Methods

Cell Culture. Fibroblasts from a male progeria patient with the 433G>A (E145K) mutation (AG10677) and from a healthy donor (AG08470; Coriell), HeLa cells, and a HeLa line expressing YFP-CENP A (from D.R. Foltz) were cultured as described in ref. 10. Transfections were carried out with the *Trans*IT-HeLa MONSTER kit (Mirus). A farnesyl transferase inhibitor FTI-277 (Sigma) was used at a concentration of 5 or 10 μM for 48-72 h. Aphidicolin (Sigma) was used at a concentration of 5 μg/mL.

Plasmids. pEGFP-C1-E145K-LA was prepared by RT-PCR amplification of the E145K-LA sequence from RNA prepared from the AG10677 cell line and ligation into pEGFP-C1; pFLAG-CMV2-E145K-LA by subcloning the E145K-LA insert from pEGFP-C1-E145K-LA into pFLAG-CMV2; and pFLAG-CMV2-WT-LA was derived from pFLAG-CMV2-E145K-LA by using the QuikChange II XL Site-Directed Mutagenesis kit (Stratagene). To construct the mCherry-myc-hLMNA vector, the LA fragment was cut from pEGFP-myc-hLMNA (32) and inserted into pmCherry-C1 (42).

Microscopy. Immunofluorescence and Hoechst staining were performed and preparations analyzed as in (11). Mouse anti-LA/C (JoL2; Chemicon), LB2 (LN43; Abcam), emerin (Novocastra), PCNA (PC10; Santa Cruz Biotechnology), FLAG (Sigma), NPC (MAb414; Covance), and rabbit anti-LA (7), LB1 (43), H3K9me3 and H3K27me3 (from T. Jenuwein), Ki-67 (DAKO), and human anti-CREST (from B. Brinkley) were used. Secondary antibodies were goat anti-mouse, anti-rabbit, and anti-human IgG-Alexa Fluor 488, 568, and 633 (Molecular Probes). Double replication labeling was carried out as in (11). Centromere and telomere localization was analyzed in z-stacks of nuclei by using Zeiss LSM software. In transfection studies, nuclear shape in 300 cells in three experiments was analyzed (mean $\pm$ SD). Live imaging was performed as in (11). Telomere FISH was carried out as described in ref. 44. For TEM, cultured cells were processed as in (45) and for negative staining as in (46). Cryo-ET and structural analysis was carried out as in (21).

Immunoblotting. Equal amounts of protein from whole cell lysates were analyzed by immunoblotting as in (11). Mouse anti-α-actin (Sigma) was used as a loading control.

In Vitro Assembly. Details are provided in *SI Text*.

ACKNOWLEDGMENTS. We thank D.R. Foltz (University of Virginia, Charlottesville, VA) for the YFP-CENP A HeLa line and D. Parry for a helpful discussion. R.D.G. was supported by the National Institute on Aging and the Ellison Foundation; H.H. by the European Commission; O.M. by the Fritz-Thysen Stiftung; H.H. and O.M. by the German-Israel Foundation; P.T. by the Sigrid Jusélius Foundation, Orion-Farmos Research Foundation, Cancer Society of Southwestern Finland, and Finnish Cultural Foundation; and K.P. by the Deutsche Forschungsgemeinschaft.

1. Dechat T, et al. (2008) Nuclear lamins: Major factors in the structural organization and function of the nucleus and chromatin. *Genes Dev* 22:832–853.
2. Stuurman N, Heins S, Aebi U (1998) Nuclear lamins: Their structure, assembly, and interactions. *J Struct Biol* 122:42–66.
3. Worman HJ, Fong LG, Muchir A, Young SG (2009) Laminopathies and the long strange trip from basic cell biology to therapy. *J Clin Invest* 119:1825–1836.
4. Hennekam RC (2006) Hutchinson–Gilford progeria syndrome: Review of the phenotype. *Am J Med Genet A* 140:2603–2624.
5. Eriksson M, et al. (2003) Recurrent de novo point mutations in lamin A cause Hutchinson–Gilford progeria syndrome. *Nature* 423:293–298.
6. Cao K, Capell BC, Erdos MR, Djabali K, Collins FS (2007) A lamin A protein isoform overexpressed in Hutchinson–Gilford progeria syndrome interferes with mitosis in progeria and normal cells. *Proc Natl Acad Sci USA* 104:4949–4954.
7. Dechat T, et al. (2007) Alterations in mitosis and cell cycle progression caused by a mutant lamin A known to accelerate human aging. *Proc Natl Acad Sci USA* 104:4955–4960.
8. Capell BC, et al. (2005) Inhibiting farnesylation of progerin prevents the characteristic nuclear blebbing of Hutchinson–Gilford progeria syndrome. *Proc Natl Acad Sci USA* 102:12879–12884.
9. Toth JI, et al. (2005) Blocking protein farnesyltransferase improves nuclear shape in fibroblasts from humans with progeroid syndromes. *Proc Natl Acad Sci USA* 102:12873–12878.
10. Goldman RD, et al. (2004) Accumulation of mutant lamin A causes progressive changes in nuclear architecture in Hutchinson–Gilford progeria syndrome. *Proc Natl Acad Sci USA* 101:8963–8968.
11. Shimi T, et al. (2008) The A- and B-type nuclear lamin networks: Microdomains involved in chromatin organization and transcription. *Genes Dev* 22:3409–3421.
12. Shumaker DK, et al. (2006) Mutant nuclear lamin A leads to progressive alterations of epigenetic control in premature aging. *Proc Natl Acad Sci USA* 103:8703–8708.
13. Van Hooser AA, Mancini MA, Allis CD, Sullivan KF, Brinkley BR (1999) The mammalian centromere: Structural domains and the attenuation of chromatin modeling. *FASEB J* 13(Suppl 2):S216–S220.
14. Aten JA, Bakker PJ, Stap J, Boschman GA, Veenhof CH (1992) DNA double labelling with IdUrd and CldUrd for spatial and temporal analysis of cell proliferation and DNA replication. *Histochem J* 24:251–259.
15. Leonhardt H, et al. (2000) Dynamics of DNA replication factories in living cells. *J Cell Biol* 149:271–280.
16. Gerdes J, et al. (1984) Cell cycle analysis of a cell proliferation-associated human nuclear antigen defined by the monoclonal antibody Ki-67. *J Immunol* 133:1710–1715.
17. Dimri GP, et al. (1995) A biomarker that identifies senescent human cells in culture and in aging skin in vivo. *Proc Natl Acad Sci USA* 92:9363–9367.
18. Tanaka H, Takenaka H, Yamao F, Yagura T (1998) Aphidicolin induces alterations in Golgi complex and disorganization of microtubules of HeLa cells upon long-term administration. *J Cell Physiol* 176:602–611.
19. Herrmann H, Aebi U (2004) Intermediate filaments: Molecular structure, assembly mechanism, and integration into functionally distinct intracellular scaffolds. *Annu Rev Biochem* 73:749–789.
20. Mücke N, et al. (2004) Molecular and biophysical characterization of assembly-starter units of human vimentin. *J Mol Biol* 340:97–114.
21. Ben-Harush K, et al. (2009) The supramolecular organization of the *C. elegans* nuclear lamin filament. *J Mol Biol* 386:1392–1402.
22. Dahl KN, et al. (2006) Distinct structural and mechanical properties of the nuclear lamina in Hutchinson–Gilford progeria syndrome. *Proc Natl Acad Sci USA* 103:10271–10276.
23. Goldfarb LG, Dalakas MC (2009) Tragedy in a heartbeat: Malfunctioning desmin causes skeletal and cardiac muscle disease. *J Clin Invest* 119:1806–1813.
24. Coulombe PA, Kerns ML, Fuchs E (2009) Epidermolysis bullosa simplex: A paradigm for disorders of tissue fragility. *J Clin Invest* 119:1784–1793.
25. Müller M, et al. (2009) Dominant cataract formation in association with a vimentin assembly disrupting mutation. *Hum Mol Genet* 18:1052–1057.
26. Wiesel N, et al. (2008) Laminopathic mutations interfere with the assembly, localization, and dynamics of nuclear lamins. *Proc Natl Acad Sci USA* 105:180–185.
27. Croft JA, et al. (1999) Differences in the localization and morphology of chromosomes in the human nucleus. *J Cell Biol* 145:1119–1131.
28. Cremer M, et al. (2001) Non-random radial higher-order chromatin arrangements in nuclei of diploid human cells. *Chromosome Res* 9:541–567.
29. Solovei I, et al. (2004) Differences in centromere positioning of cycling and postmitotic human cell types. *Chromosoma* 112:410–423.
30. Weierich C, et al. (2003) Three-dimensional arrangements of centromeres and telomeres in nuclei of human and murine lymphocytes. *Chromosome Res* 11:485–502.
31. Cowan CR, Carlton PM, Cande WZ (2001) The polar arrangement of telomeres in interphase and meiosis. Rabl organization and the bouquet. *Plant Physiol* 125:532–538.
32. Moir RD, Yoon M, Khuon S, Goldman RD (2000) Nuclear lamins A and B1: Different pathways of assembly during nuclear envelope formation in living cells. *J Cell Biol* 151:1155–1168.
33. Dechat T, et al. (2004) LAP2alpha and BAF transiently localize to telomeres and specific regions on chromatin during nuclear assembly. *J Cell Sci* 117:6117–6128.
34. Glass JR, Gerace L (1990) Lamins A and C bind and assemble at the surface of mitotic chromosomes. *J Cell Biol* 111:1047–1057.
35. Burke B, Gerace L (1986) A cell free system to study reassembly of the nuclear envelope at the end of mitosis. *Cell* 44:639–652.
36. Lopez-Soler RI, Moir RD, Spann TP, Stick R, Goldman RD (2001) A role for nuclear lamins in nuclear envelope assembly. *J Cell Biol* 154:61–70.
37. Luderus ME, den Blaauwen JL, de Smit OJ, Compton DA, van Driel R (1994) Binding of matrix attachment regions to lamin polymers involves single-stranded regions and the minor groove. *Mol Cell Biol* 14:6297–6305.
38. Schmitt J, et al. (2007) Transmembrane protein Sun2 is involved in tethering mammalian meiotic telomeres to the nuclear envelope. *Proc Natl Acad Sci USA* 104:7426–7431.
39. Scaffidi P, Misteli T (2005) Reversal of the cellular phenotype in the premature aging disease Hutchinson–Gilford progeria syndrome. *Nat Med* 11:440–445.
40. McClintock D, Gordon LB, Djabali K (2006) Hutchinson–Gilford progeria mutant lamin A primarily targets human vascular cells as detected by an anti-Lamin A G608G antibody. *Proc Natl Acad Sci USA* 103:2154–2159.
41. Scaffidi P, Misteli T (2008) Lamin A-dependent misregulation of adult stem cells associated with accelerated ageing. *Nat Cell Biol* 10:452–459.
42. Vignjevic D, et al. (2006) Role of fascin in filopodial protrusion. *J Cell Biol* 174:863–875.
43. Moir RD, Spann TP, Goldman RD (1995) The dynamic properties and possible functions of nuclear lamins. *Int Rev Cytol* 162B:141–182.
44. Solovei I, et al. (2002) Spatial preservation of nuclear chromatin architecture during three-dimensional fluorescence in situ hybridization (3D-FISH). *Exp Cell Res* 276:10–23.
45. Starger JM, Brown WE, Goldman AE, Goldman RD (1978) Biochemical and immunological analysis of rapidly purified 10-nm filaments from baby hamster kidney (BHK-21) cells. *J Cell Biol* 78:93–109.
46. Foeger N, et al. (2006) Solubility properties and specific assembly pathways of the B-type lamin from *Caenorhabditis elegans*. *J Struct Biol* 155:340–350.